Controlling morphology using low molar mass nucleators

Chapter 5

Controlling Morphology using Low molar mass nucleators

Geoffrey R Mitchell,[1] Supatra Wangsoub,[2] Aurora Nogales[3], Fred J Davis[4] and Robert H Olley[5]

[1] Centre for Rapid and Sustainable Product Development, Institute Polytechnic of Leiria, Marinha Grande Portugal
[2] Department of Chemistry, Naresuan University, Thailand
[3] Instituto de Estructura de la Materia, CSIC, Madrid Spain.
[4]Department of Chemistry, The University of Reading, Whiteknights, Reading, RG6 6AD, UK
[5]Electron Microscopy Laboratory, The University of Reading, Whiteknights, Reading, RG6 6AF, UK

5.1 Introduction

Crystallisation is a hugely important process in physical sciences and is crucial to many areas of, for example, chemistry, physics, biochemistry, metallurgy and geology. The process is typically associated with solidification, for example in the purification of solids from a heated saturated solution familiar to all chemistry undergraduates. Crystalline solids are also often the end result of cooling liquids, or in some cases gases, but in order to form require nucleation, in the absence of nucleation supercoiling of liquids well below the melting point is possible (Cavagna, 2009). The quality of crystals, as gauged by size and levels of order is highly variable, and may depend on factors such as material purity and the rate of cooling; rapid cooling may result in poor crystallisation, or even the formation of amorphous materials with no long range order. In geological systems rates of cooling may vary over many orders of magnitude, for example obsidian is a largely amorphous material produced when lava is rapidly cooled (Tuffen, 2003), while the gypsum crystals found in the Cueva de los Cristales in Chihuahua, Mexico can reach 10 metres in length (Figure 1) and are formed over hundreds of thousands of years. In this latter case the formation of such large spectacular structures as shown in Figure 1 can only be explained by a low nucleation rate (García-Ruiz, 2007; Van Driessche, 2011).

Figure 5.1*: Giant gypsum crystals in the Cueva de los Cristales in Chihuahua, Mexico, the scale is indicated by the person (photo A. Van Driessche)*

Crystallisation from solution is a core technology in major areas of the chemical industry and it is the critical initial step in many scientific programmes including structural studies of proteins and pharmaceuticals. The process of nucleation by which embryonic crystals form within a supersaturated solution remains largely unexplained. In classical nucleation theory, the volume excess free energy of the nuclei at a critical radius balances the surface excess free energy; nuclei larger than this critical radius grow, smaller entities dissolve back in to the solution. Recently other pathways of transformation have been identified theoretically in which structure and density fluctuations are separated (Kashchiev, 2005). In terms of controlling morphology in polymers, nucleation of polymer crystals plays an important part in the production of several commodity plastics giving the potential for control of the polymer microstructure and therefore the subsequent properties (Bassett, 2006). Nucleating agents are thus of considerable commercial and scientific interest. One well known example of a nucleating agent is 1,3:2,4-dibenzylide sorbitol (I) (DBS); this is extensively used as a clarification agent with polypropylene. Its use leads to transparent materials with improved mechanical properties (Zweifel, 2001). This chapter focuses on the use of nucleating agents to control the structure and morphology of polymers and focuses particularly on DBS and its derivatives (Nogales et al 2005, Nogales et al 2016). In particular the work describes the self-assembly of such materials to form a template which can direct the crystallisation of polymers such as poly(ε- caprolactone).

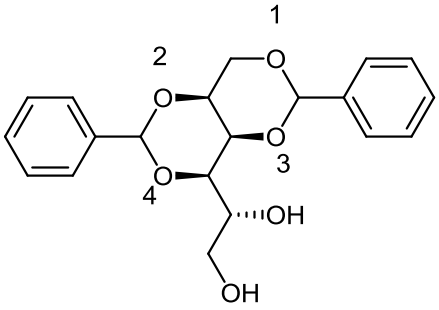

(5.1)

5.2 Organic Gelators

In general, gels are viscoelastic solid-like materials comprised of an elastic cross-linked network and a solvent, which is the major component. The solid-like appearance of a gel is a result of the entrapment and adhesion of the liquid in the large surface area solid 3D matrix. DBS (Scheme 5.1) is an example of a low molar mass organic gelator (Terech, 1997); that is a gel derived from low molar mass compounds formed through self-aggregation of the small gelator molecules to produce entangled self-assembled fibrils (Smith, 2009; Sangeetha, 2005). In the case of DBS typically these fibrils are of the order of about 10 nm in diameter and at sufficiently high DBS concentrations (generally less than 2wt% depending on factors such as temperature and matrix polarity), the nanoscale fibrils form a three dimensional network that promotes physical gelation in a wide variety of organic solvents and polymers.

The structures and properties of DBS-organogels formed in different solvents are well studied by Yamasaki and Tsutsumi (Yamasaki, 1994, 1995 a,b; Watase, 1998). All of those studies show that DBS builds up helically twisted fibres in low viscosity solvents. This is accompanied by a tremendous change in the rheological properties of these materials, if self-assembling leads to gelation. This gelation is based on physical interaction between the molecules. Gelation depends on various factors, such as gelator concentration, temperature, and solvent polarity. It has also been shown (Yamasaki, 1995a) that the DL-racemate is not able to self-aggregate; thus, chirality seems important in the self-organisation of DBS (though it might be expected that the L-enantiomorph would assemble in a similar-form). Wangsoub et al 2016 have reported the properties and structure of gels formed from alkanes and dibenzylidene sorbitol, the results are relevant in part to the use of DBS with polyethylene

Gels of a low molecular mass compounds are usually prepared by heating the gelator in an appropriate solvent and cooling the resulting isotropic supersaturated solution to room temperature. When the hot solution is cooled, the molecules start to condense and three situations are possible Figure 5.1: (1) a highly ordered aggregation giving rise to crystals i.e. crystallisation (2) a random aggregation resulting in an amorphous precipitate or (3) and aggregation process intermediate between these two yielding a gel (1). The process of gelation involves self-

association of the gelator molecules to form long, polymer-like fibrous aggregates, which get entangled during the aggregation process forming a matrix that traps the solvent mainly by surface tension. This process prevents the flow of solvent under gravity and the mass appears like a solid. At the microscopic level, the structures and morphologies of molecular gels have been investigated by conventional imaging techniques such as SEM, TEM and AFM. At the nanoscale, X-ray diffraction, small angle neutron scattering and X-ray scattering (SANS, SAXS) are required to elucidate the structures of molecular gel.

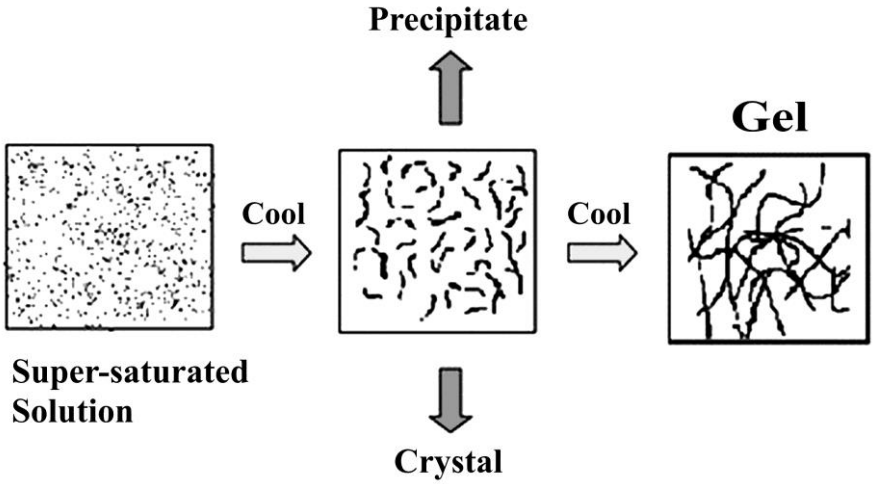

Figure 5.2 Schematic representation of aggregation modes (redrawn after Sangeetha and Maitra, 2005).

5.3 Synthesis of Sorbitol Derivatives

D-Sorbitol, or D-glucitol is a sugar alcohol that is produced commercially by the reduction of glucose, but is also found naturally in many fruits. It finds many uses as an ingredient in the food industry and as such is designated E420 (Hanssen and Marsden 1984), though its use has been tainted with problems such as diarrhoea and flatulence. The dibenzylidene derivative is the main product of treatment with benzaldehyde, though mono and trisubstituted byproducts may also be formed. Degradation and other studies confirmed that it is the 1,3:2,4 diacetal that is formed (Okesola, 2015). A range of other derivatives can be readily formed by the acid catalysed reaction of sorbitol with the appropriate substituted aldehyde (e.g. benzaldehyde, benzaldehyde d_6, or 4-chlorobenzaldehyde) in cyclohexane (Wangsoub, 2008). A typical procedure, that for 1,3:2,4-di(4-chlorobenzylidene) sorbitol (Scheme 5.2) was as follows. An aqueous solution of D-sorbitol (0.1 mol, 70% w/v) was placed into a round bottom flask equipped with Dean-Stark trap

and condenser. To this was added 4-chlorobenzaldehyde (0.2 mol) and methanesulfonic acid (1 ml), cyclohexane (200 mL) and dimethylsulfoxide (6 mL). The mixture was heated to reflux with constant stirring. The mixture of cyclohexane and water was condensed and separated in the Dean-Stark arrangement. Once no further water was produced the reaction was stopped, and following neutralisation with triethylamine the white precipitate collected. Following purification by washing with dioxane and water 1,3:2,4-di(4-chlorobenzylidene) sorbitol was obtained as a white powder. The product was greater than 98% pure by ^{1}H NMR, yield 19.7g, 46 %, m.pt. 187°C.

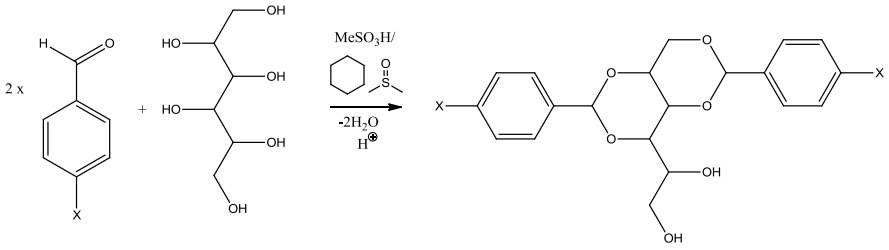

Scheme 5.2: *Synthesis of Sorbitol derivatives*

5.4 DBS in Polymers

DBS and its derivatives can be easily dispersed in polymers using either melt mixing or mixing using a common solvent and drying. For the results shown here, the latter approach was used due to the small volume of material required. In this work we used the shear flow cell (Nogales et al 2004) shown in Chapter 3 (Figure 3.22) and for this, samples were prepared by co-solvent mixing, for example with PCL we employed butanone, drying and then melt pressing in to discs.

Figure 5.3 shows the phase behavior of the Cl-DBS/PCL system (Wangsoub et al 2008). The line for the crystallisation temperature shows that the addition of the Cl-DBS increases the crystallisation temperature by ~^10ºC due to the nucleating effect of the DBS derivative. This effect saturates at 1% with Cl-DBS/PCL in contrast to ~3% for DBS/PCL (Wangsoub, Olley and Mitchell 2003). The upper curve shows the liquidus line separating the high temperature homogenous melt from the lower temperature 2 phase state of molten PCL and crystalline Cl-DBS fibrils. The liquidus line is shifted upwards by ~20ºC from the equivalent line for the DBS/PCL system (Wangsoub, Olley and Mitchell 2005) indicating a reduced solubility for Cl-DBS in PCL.

The phase behavior of the DBS or DBS derivative is dependent on both the chemical nature of the additive and the polarity of the polymer. For example with DBS in PCL, the nucleating effect saturates at ~3% whereas in polyethylene it saturates at a much lower concentration (Nogales , Olley and Mitchell .2005)

Figure 5.4 shows the results of a cooling experiment from the single homogenous phase of a composition of 3% Cl-DBS in PCL in which we plot the invariant (equation 1) calculated from the SAXS patterns recorded in a time-resolved manner. Each SAXS pattern was recorded as a 2d dataset I(Q,α). The invariant Ω was calculated using Equation 5.1 (Mitchell 2013):

$$\Omega = \int_0^{\pi/2} \int_{Q=0}^{Q_{max}} \left|\underline{Q}\right|^2 I(\left|\underline{Q}\right|, \alpha) \sin\alpha dQ d\alpha$$

Eqn 5.1

The invariant is related to the average of the electron density differences and for example in the early stages of crystallization, it is proportional to the volume of crystals. In Equation 5.1, Q is the scattering vector, whose magnitude is given by $4\pi\sin(\theta)/\lambda$, where 2θ is the scattering angle and λ is the wavelength of the incident x-rays. α is the angle between a specific direction and the scattering vector.

Initially the invariant has a low value and falls slightly with reduced temperature. At T ~127ºC, the invariant increases sharply and this corresponds to formation of nanofibrils. Eventually at lower temperatures the invariant plateaus and slightly falls. When the temperature reaches 40ºC there is a second increase in the invariant which corresponds to the crystallization of the PCL. It is clear that these two different ordering processes occur quite separately from each other. We can obtain more information about the state of the Cl-DBS in the 2 phase region by subjecting the material to a shear flow which leads to alignment of the Cl-DBS fibrils.

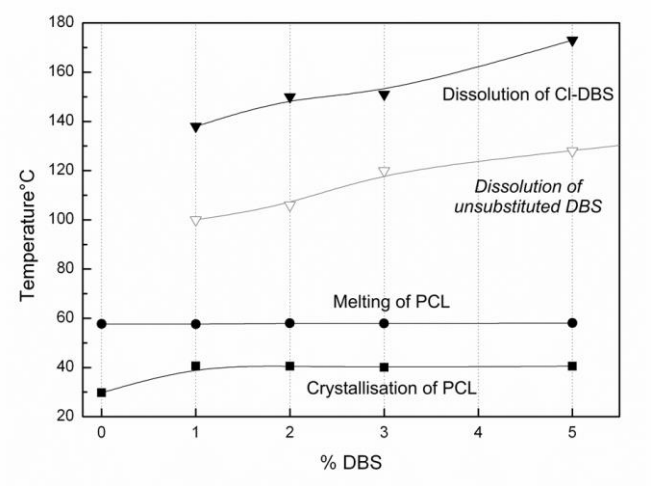

Figure 5.3 A part of the phase diagram for the PCL, Cl-DBS system with the liquidus line for Cl-DBS/PCL (▼) *and the liquidus line for DBS/PCL (∇), PCL melting point* (●) *and the PCL crystallization*

temperature on cooling from the single phase melt (■). Redrawn from Wangsoub et al 2008)

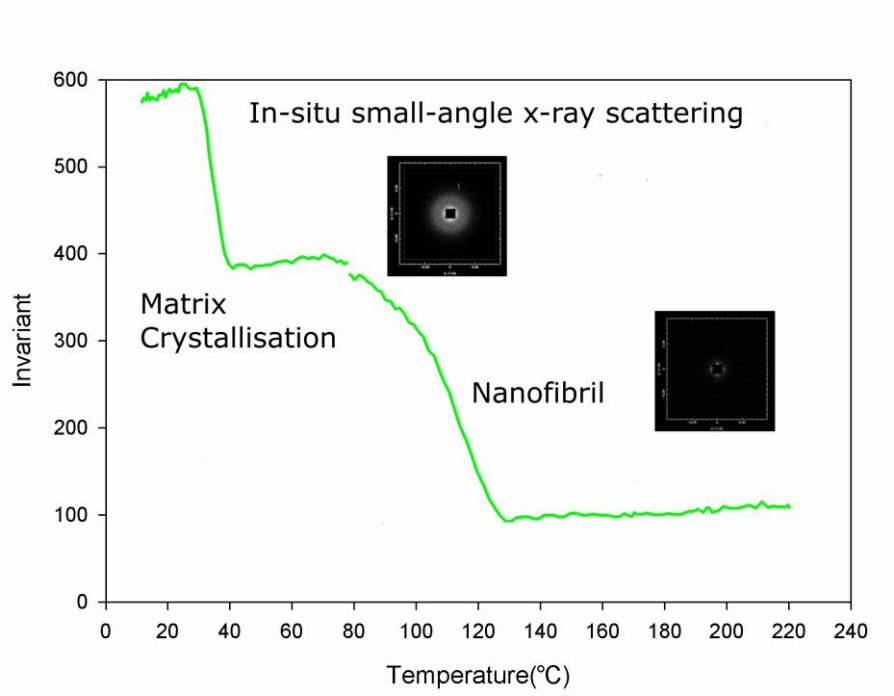

Figure 5.4 A plot of the SAXS invariant Ω, (Equation 1) obtained from a sequence of time-resolving SAXS patterns recorded whilst cooling a 3% Cl-DBS/PCL system from the higher temperature single phase region to Room Temperature at 10°C/min. (Redrawn from Mitchell 2013) The insets show SAXS patterns taken at the temperatures corresponding to their position on the temperature scale.

Figure 5.7a shows the SAXS pattern recorded in the 2-phase region. The horizontal streak corresponds to highly anisotropically shaped objects aligned parallel to the shear flow direction. Analysis of this scattering shows that it arises from objects with a radius of ~14nm and a length great than 100nm. (Wangsoub and Mitchell 2009). It is clear that a high level of anisotropy of these objects is achieved at modest shear rates. The level of anisotropy that can be achieved will also depend on the polymer and its molecular weight distribution.

polymer	Mw	Mn	Mv	Type
Polymer Code	Mw	Mn	Mv	Type
PE190	18,700	5,410	10,000	Linear
GA	70,950	6,250	45,000	Linear
GX	163,100	17,650	105,000	Linear
PE26	424,150	97,650	350,000	Linear

Table 1 Molecular weight Characteristics of Polymers used in the experimentals reported in Figure 5.5

Wangsoub et al have reported the effects of the molecular weight distribution in the Polyethylene/DBS system (Wangsoub et al 2016). Samples were subjected to the same shear/temperature profile of 1,000 shear units at $10s^{-1}$ at temperatures considerably higher than the melting point of each material. After cooling to room temperature at 10ºC/min the samples were examined using wide-angle x-ray scattering and the azimuthual profiles for the 110 reflection are shown in Figure 5.5. The lowest 2 molecular weight matrix polymers, PE190 and GA show only a modest level of anisotropy as judged from the small variation in intensity with azimuthual angle, whereas the highest 2 molecular weight matrix polymers, GX and PE26 show a marked level of anisotropy. We attribute this to the stress which develops during shearing in the melt and its effect of the orientation of the DBS fibrils. In the curve for 1%DBS/PE26, the high molecular weight matrix polymer, there is evidence for a range of lamellar tilt angles, in the form of a four point pattern which is usually occurs when the matrix polymer is under stress in the typical shish kebab structures (Pople et al 1999, Olley et al 2014)).

We have tested the effect of the DBS on the long period of the polyethylene GX and as Figure 5.6 shows for samples crystallized at different temperatures the long period for GX alone or GX/DBS are essentially the same. In other words the role of the DBS is to direct the crystallization of the polymer, the lamellar structure remaining unaffected.

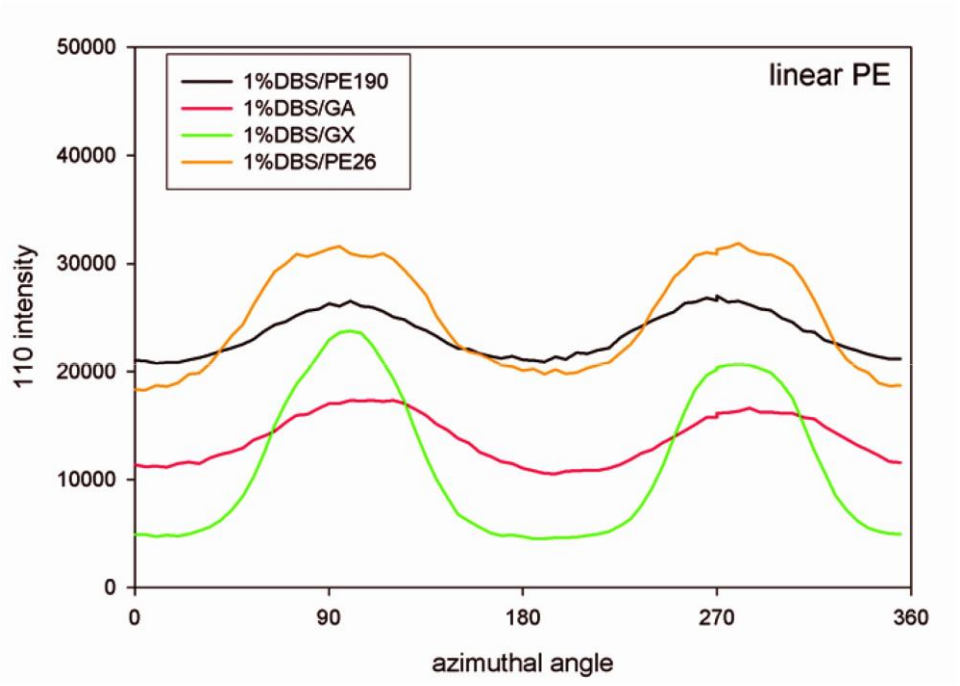

Figure 5.5 WAXS Azimuthal profiles for the 110 reflection in Linear Polyethylene samples with different molecular weight distributions as listed in Table containing 1% DBS crystallized from a sheared melt as described in the text.

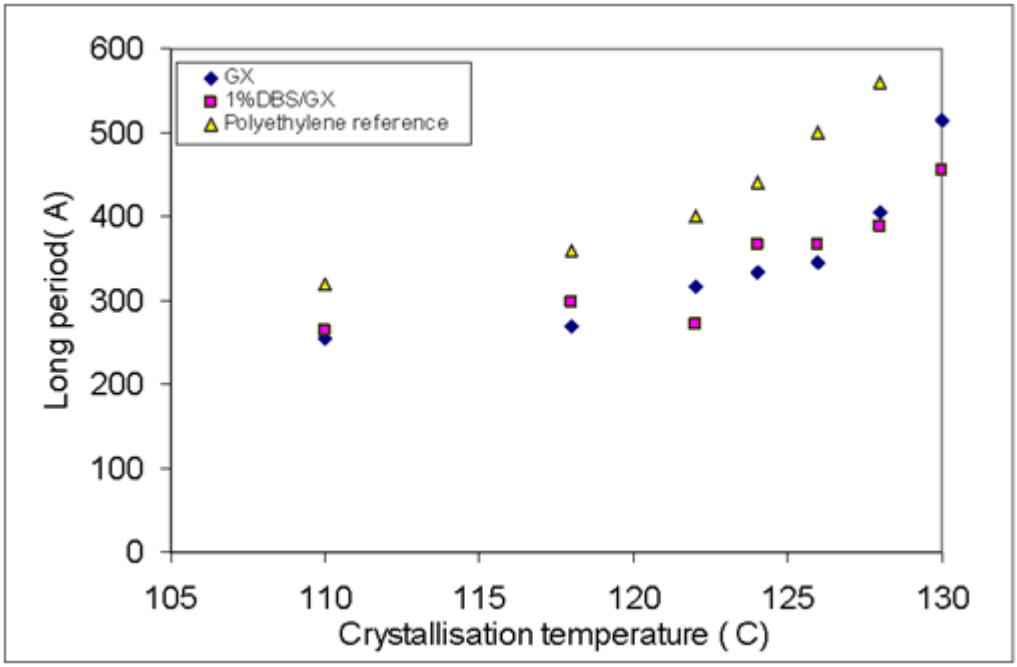

Figure 5.6 The long periods for a series of polyethylenes crystallized at differing temperatures for Polyethylenes GX with and without DBS as indicated in the key.

Figure 5.7b shows the WAXS pattern for the equivalent system to that shown in Figure 5.7a. The figure is a difference between the pattern recorded in the 2 phase region and that recorded in the homogenous high temperature phase. As the scattering from the molten polymer and the crystallized DBS will be additive, we can subtract the polymer scattering to give a clearer view of the pattern of the additive.

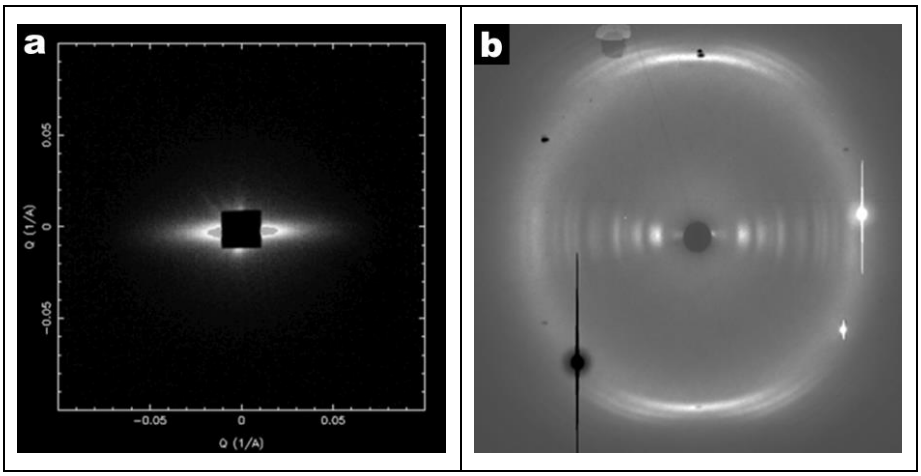

Figure 5.7 (a) SAXS and (b) WAXS patterns recorded for a sample of Cl-DBS/PCL during shear flow 10s-1 in the 2 phase region of the phase diagram.

It is clear that the Cl-DBS exhibits an ordered crystalline phase. It is interesting that the DBS fibrils are crystalline. This gives them different physical characteristics to other fibrillar gel systems such as self-assembling polypeptide gels and the worm-like micellar systems. The crystal structure leads to very rapid crystal growth in one direction, whereas in the lateral direction, the crystal growth is slower and more fragile. As discussed elsewhere this may be a consequence of the chiral nature of the structures. Optical microscopy studies have shown that the DBS nucleates crystallization of the DBS from the single phase melt of polymer and DBS. Shear flow may lead to breakage of fibrils whereas the self-assembled micellar systems are virtual polymers and can pass through each other by breaking and reforming. There is good experimental evidence that shear flow leads to some breakage of fibrils. Of course reheating to the single phase region and subsequent crystallization would lead to repair but loss of any anisotropy which had developed.

Prolonged shearing of the system shown in Figure 5.7 leads to some unexpected changes. The sequence of SAXS patterns in Figure 5.8 shows the effect increasing shear strain. We attribute the appearance of additional peaks in the pattern to a narrowing of the fibril diameter distribution. We have analyzed the results using a Monte Carlo methodology to fit to Gaussian Distribution of Cylinder radii (Wangsoub and Mitchell 2009). The extracted results are shown in Figure 5.9 with plots of the mean radius which is largely unchanged and the Gaussian radius distribution b. The width reduces sharply a reaches a plateau value between 5000 and 10000 shear units (shear rate × time of shearing).

Of other sugar alcohols, debenzylidene xylitol is widely used as a gelling agent; moreover the three enantiomeric carbons in xylitol are arranged like a sequence of three carbons in xylitol. Dibenzylidene xylitol has been specified in the literature as a nucleating agent for polymers, but was not found to have any significant directing effect in polypropylene or polycaprolactone.

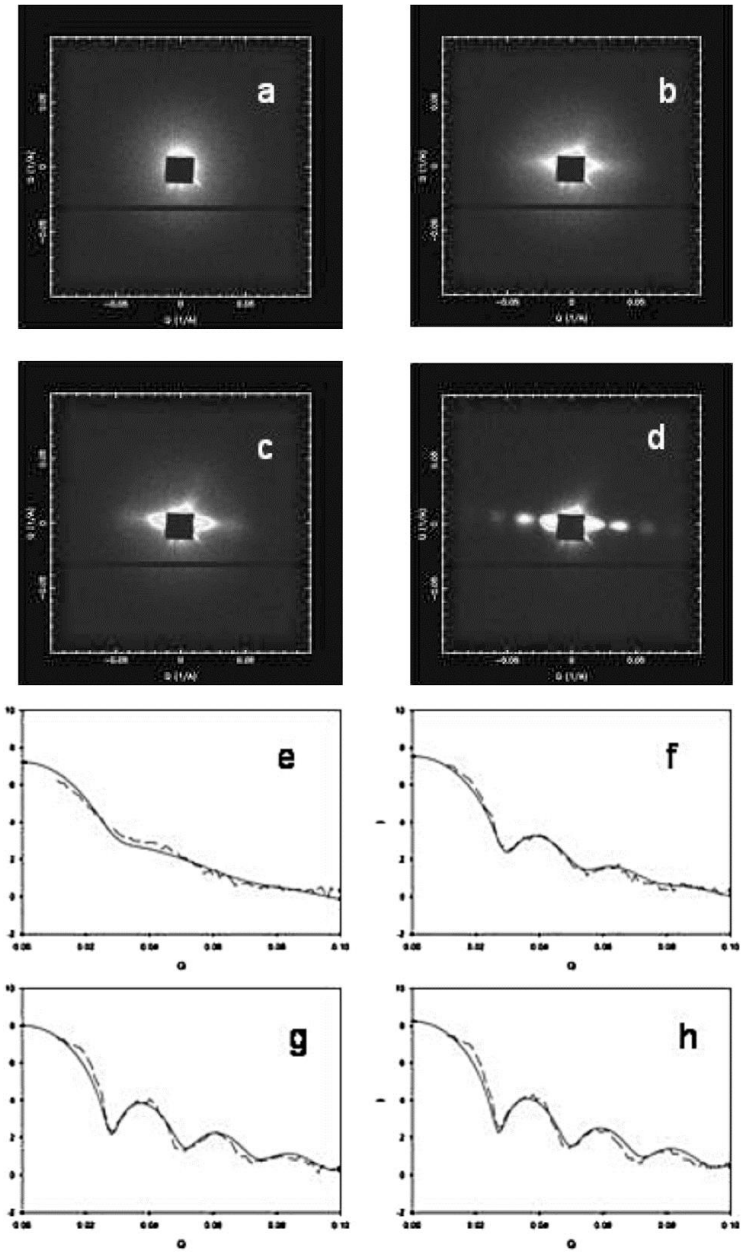

Figure 5.8 Selected SAXS patterns corresponding to shear strains of (a) 0, (b) 100 su, (c) 10,000 su and (d) 28,000; e-h Equatorial sections (broken lines) corresponding to shear strains of (e) 1,000 su (f) 4,000 su, (g) 13,000 su and (h) 28,000 su taken from patterns from the same series as shown in a-d but for the shear strains indicated. The full lines in the sections correspond to the best-fit model for a set of polydisperse cylinders. The fitting parameters are plotted in Figure 5.9.

The horizontal black bar in the lower half of each pattern arises from a defect in defect in the detector system during the measurements.

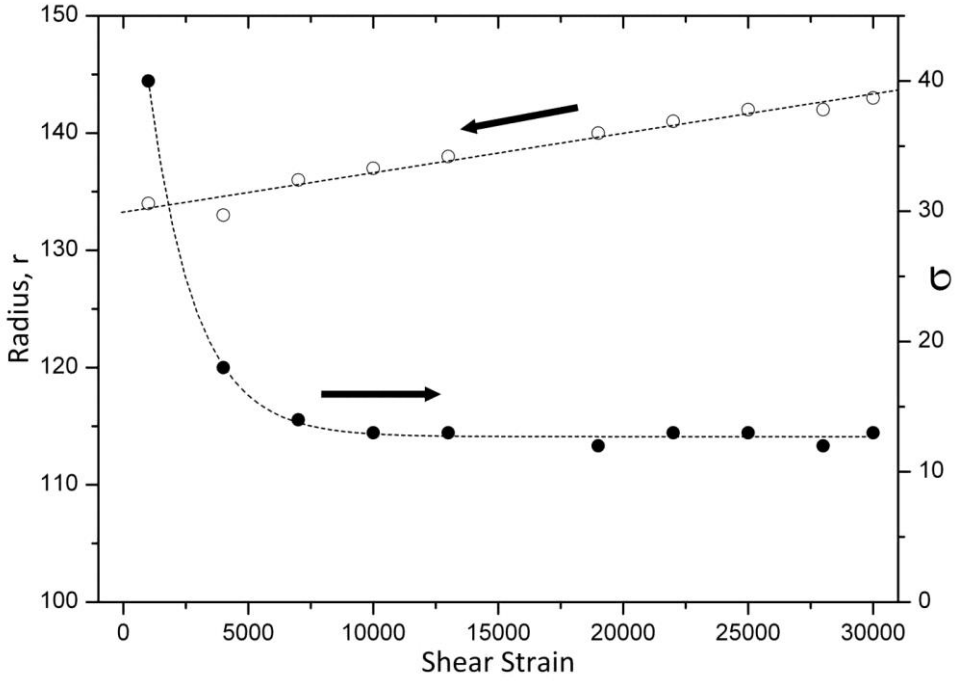

Figure 5.9 Plots of the mean diameter and the standard deviation of the Gaussian radius distribution as a function of increasing shear strain obtained from SAXS data using a Monte Carlo approach. Re-drawn from Wangsoub and Mitchel 2009)

In contrast to the generation of row nuclei in polymers with a high molecular weight tail in the distribution, cessation of shear flow does not immediately lead to the relaxation of the oriented row nuclei. The aligned DBS fibrils remain aligned for quite some period (hours) which will doubtless is some cases lead to difficulty with experiments whilst attempting to remove prior history. Of course it may also prompted some novel methods of developing the anisotropy.

5.5 DBS Directing Crystallisation

We have shown in 5.4 how by using shear flow in conjunction with a polymer containing a DBS derivative we can obtain aligned nanoscale fibrils which are arranged parallel to the shear flow. This can be achieved while the matrix polymer is in the molten state. If we now crystallise the sample we can exploit these extended objects as row nuclei to direct the crystalline morphology of the matrix polymer. Figure 5.10 shows a SAXS pattern recorded at Diamond on beamline I22 using the shear flow cell with Cl-DBS/PCL sample, after a cycle of shearing

and cooling. The horizontal streak around the beam stop corresponds to the highly extended fibrils about 14-15nm radius and greater than 100nm long. The features above and below the beam stop are typical of small-angle scattering from semi-crystalline polymers and relate to the lamellar crystal morphology. Clearly the level of preferred orientation of both the nanofibrils and the crystal lamellae is very high.

Figure 5.11 shows the same type of information but revealed using electron microscopy coupled with differential etching. The extended object in the centre of the image is the impression of the DBS fibrils left in the polymer matrix after it was removed by etching. We can see that the main object is made up of smaller fibrils fused together. The highly aligned lamellae , seen here edge on, are easily visible and their geometric arrangement to the DBS nanofibrils is clear. In the following two images the directing influence of the DBS nanofibrils can be easily observed. In Figure 5.9b to the left beyond the end of the impression left by the nanofibril we can see a more random arrangement of lamellae. In fact we can now see some face on. Furthermore between the two nanofibrils which are not quite parallel with each other we can the two sets of directed lamellae impacting in the centre portion.

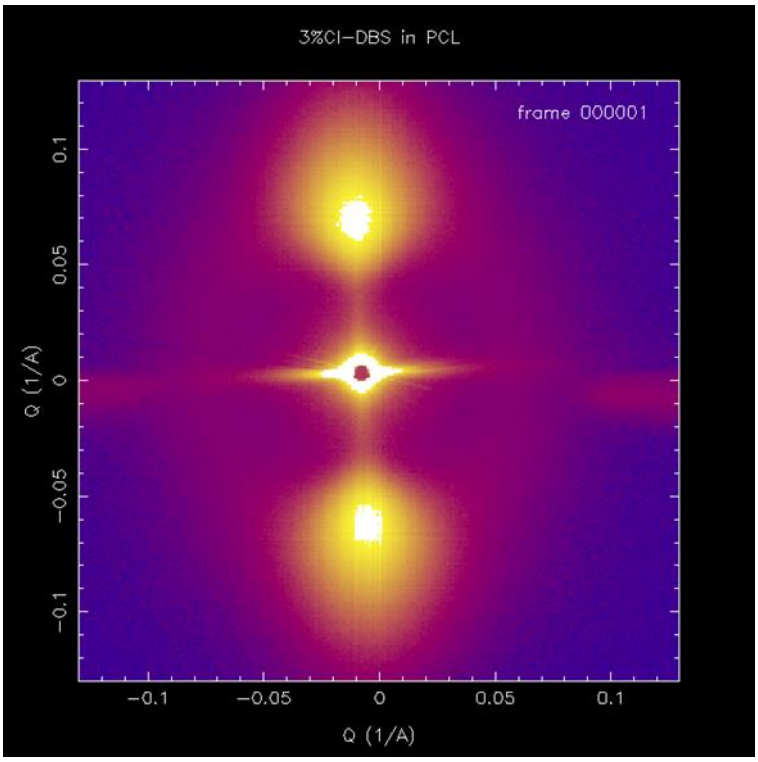

Figure 5.10 shows the SAXS pattern recorded for the 3% Cl-DBS/PCL system after shearing at 80°C at a shear rate of $10s^{-1}$ This

pattern was obtained at the Diamond Light Source beam line I22 (redrawn from Mitchell 2013)

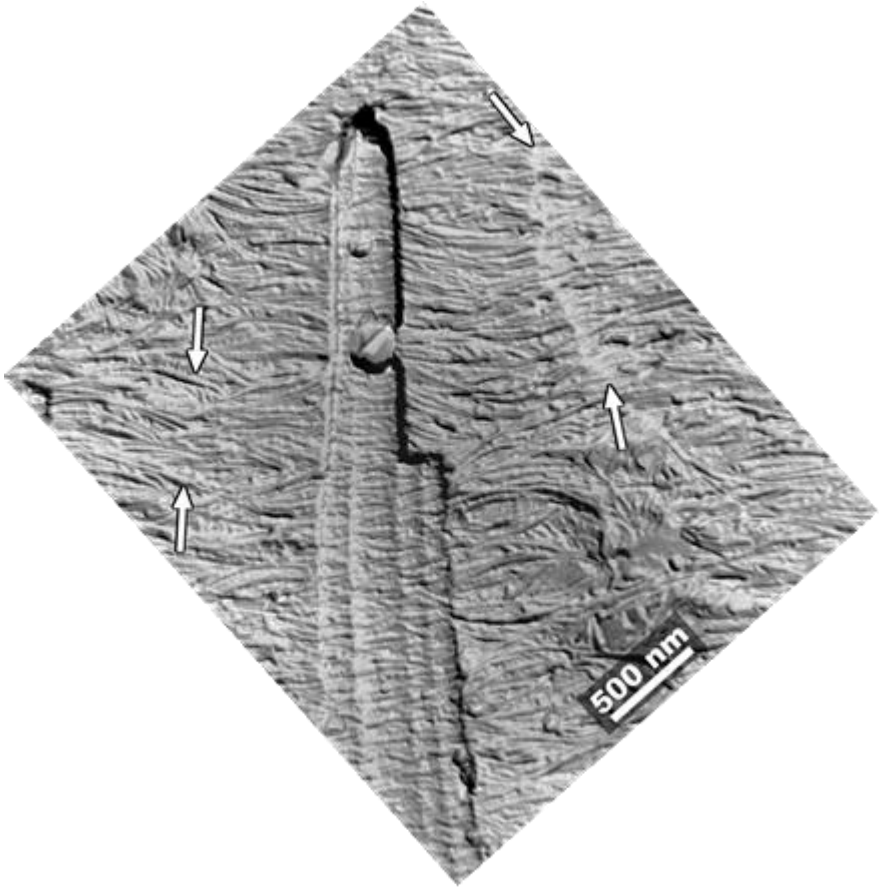

Figure 5.11 Transmission electron micrograh of a replica of a differentially etched interior surface of polyethylene sample containing DBS.

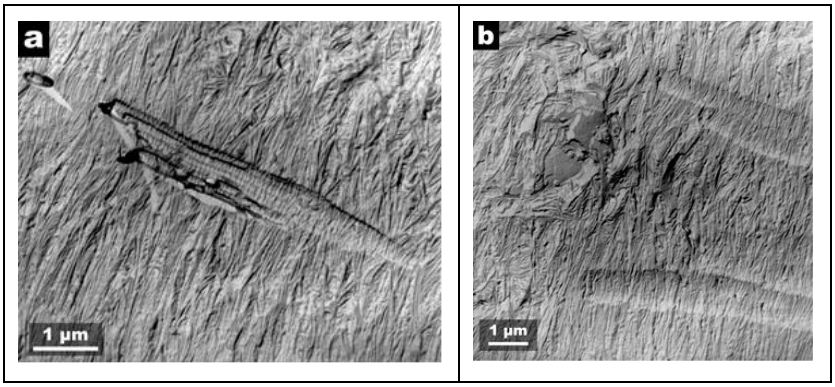

Figure 5.12 (a) Detail of a single cluster of DBS fibres (b) Polyethylene development from DBS fibres, right, compared with general development, left.

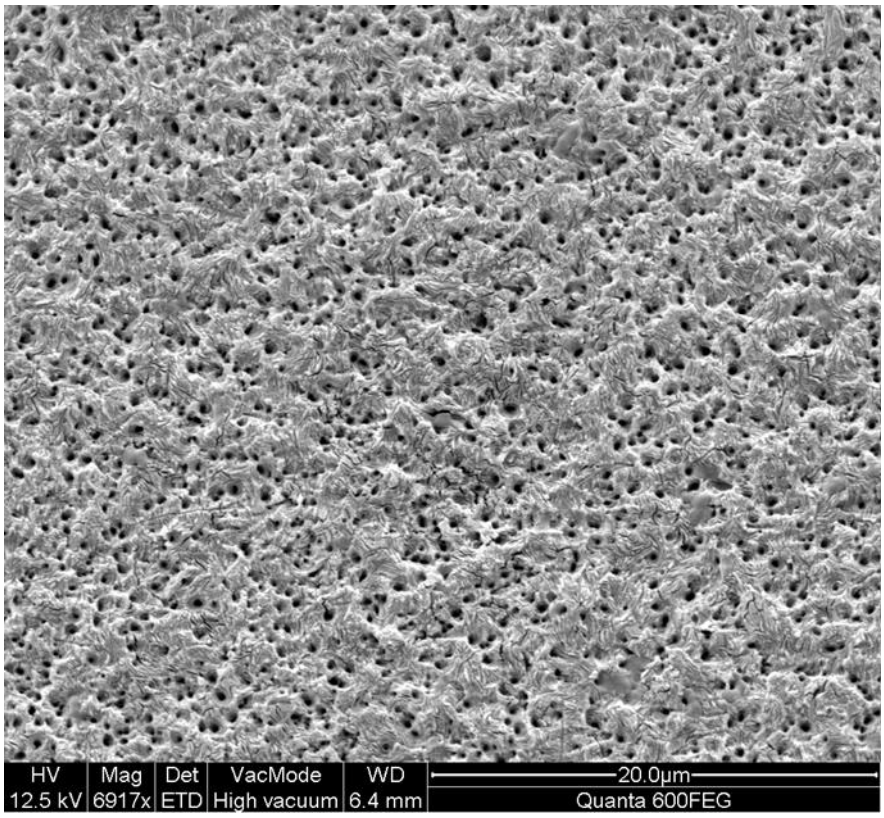

Figure 5.13 A scanning electron micrograph of the surface of section cut through a sheared disc which was crystallised from a sheared melt of PE/DBS. The surface is perpendicular to the alignment of the DBS fibrils.

Figure 5.13 shows the interior surface of DBS/PE system [] prepared by cutting a sheared disc in half. We are now looking in a direction parallel to the aligned nanofibrils. The holes correspond to where the nanofibrils were, and subsequent etching has broaden the hole from its original size. We can see the excellent dispersion of the DBS nanofibrils.

5.7 Model of Directed Crystallisation

In the case of highly aligned fibrils, consideration of the templating process reduces to a 2-d matter. The number density of fibrils is given by (Wangsoub et al 2008)

$$N = (f - f_c) \Big/ \pi r_f^2$$

where f is the fraction of the additive and f_c is the upper limit of solubility of the additive in the polymer matrix. We consider all fibrils to have the same radius r_f.

If we associate a templated zone of radius r_t with each fibril the fraction of templated material, f_t, (Figure 5.14) is given by:

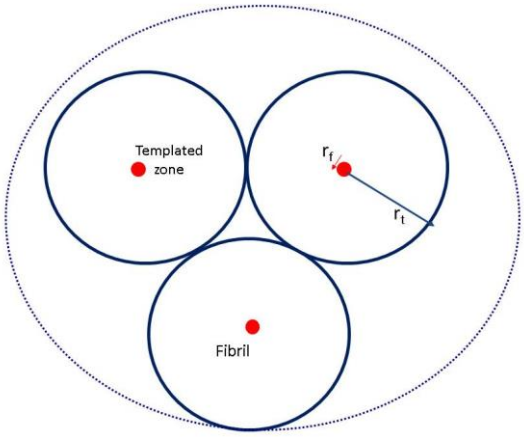

Figure 5.14

$$f_t = (f - f_c)\frac{\pi r_t^2}{\pi r_f^2}$$

Clearly this is a very simple model without any distribution of fibril dimensions and the templated zone size does not account for a random spatial distribution of fibrils. However, we do have an estimate of the fibril radius of ~7.5nm from the SAXS measurements and we have estimated for polyethylene that the templated zone has a radius ~100nm. This suggests that the value of ($f - f_c$) needs to be greater than 0.014 to achieve full templating. Clearly the solubility of the sorbitol derivative in the polymer matrix is critical in determining the actual amount of additive required to achieve this. We previously estimated that the solubility limit of DBS in PCL was ~0.01 and we attribute in large part the enhanced templating of Cl-DBS to a reduction in the solubility limit in PCL. This is shown in the DSC and liquidus line In the examples of the morphology shown in Figure 5.8 to 5.10, the directing is more or less perfect and the hence the orientation parameter $<P_2>_L$ describing the preferred orientation of the lamellae with respect to the flow axis is given by the fraction of material templated:

$$< P_2 >_L = -0.5(f - f_c)\frac{\pi r_t^2}{\pi r_f^2}$$

The factor –0.5 (Lovell and Mitchell 1981) takes account of the fact that the lamellae are arranged normal to the flow axis. The efficacy of the templaating or

directing process depends on the number density of the DBS fibrils. For a given amount of DBS, the number density can be optimized by making the nanofibrils as thin as possible. The processes described in this chapter are effective because of the lateral nanoscale of the fibrils.

5.6 Summary

We have shown that the inclusion of small amounts of DBS or selected derivatives leads to the formation of a well dispersed system of nanofibrils. These are particularly effective in directing the crystallization of polyethylene, polypropylene and poly(ε-caprolactone) due to the high number density of the fibrils in the sample.. It may well be possible to extend to other polymer systems. Such work is underway. The approach offers distinct advantages over the other approaches described in other chapters in this volume. It avoids the use of viscous high molecular fractions to produce row nuclei. By using a nanoparticle it may be possible achieve other orientations of the nanoparticles than parallel to the flow axis. The latter takes place because of the high level of anisotropy of the nanofibrils. The high aspect raio of the nanofibrils means that any deformation of the polymer melt is likely to lead to a high level of orientation of the nanofibrils leading to a high level of preferred orientation of the lamellar crystals

5.7 Acknowledgements

This work was supported by the Fundação para a Ciência e a Tecnologia (Portugal) through project PTDC/CTM-POL/7133/2014 and through the Project reference UID/Multi/04044/2013

We thank Naresuan University for supporting SW during her PhD programme and the Faculty of Science at Naresuan University for funding subsequent short visits when much of the work described here was performed.

This chapter contains various data recorded at international synchrotron and neutron scattering facilities. We are indebted to those facilities for access and to the beamline scientists for their involvement in these experiments. Dr Sigrid Bernstoff (Elettra) , Dr Francois Fauth (ESRF), Dr Sergio Funari (Hasylab), Dr Jen Hiller and Dr Nick Terrill (Diamond), Dr Steve King, Dr Sarah Rogers, Dr Ann Terry, Dr Richard Heenan (ISIS)

5.8 References

Bassett DC (2006), Linear nucleation of polymers, *Polymer*, 47, 5221–5227

Cavagna A. (2009),Supercooled liquids for pedestrians *Physics Reports* , 476 (4–6), 51–124.

García-Ruiz JM, Villasuso R, Ayora C, Canals A, Otálora F. (2007, Formation of natural gypsum megacrystals in Naica, Mexico, Geology, 35(4) 327–330

Grubb DT, Dlugosz J., Keller A. (1975) Direct observation of lamellar morphology in polyethylene Journal of Materials Science 10, 1826-1828

Hanssen M and Marsden J. (1984), E for Additives, The complete number guide,

Kashchiev D, Vekilov PG and Kolomeisky AB. (2005), Kinetics of two-step nucleation of crystals, *J Chem. Phys*. 122 244706.

Lovell R. and Mitchell G.R. (1981) Molecular Orientation Distribution Derived from an Arbitary Refelection Acta Cryst A37 135-137

Mitchell G.R. Characterisation of safe nanostructured polymers in Ecosustainable Polymer nanomaterials for food packaging Edited by Clara Silvestre and Sossio Cimmino Taylor and Francis January 2013 Print ISBN: 978-90-04-20737-0 eBook ISBN: 978-90-04-20738-7

Nogales A. and Mitchell G.R. (2005) Development of highly oriented polymer crystals from row assemblies *Polymer* **46** 5615-5620

Nogales A., Olley R.H. and Mitchell G.R. (2003) Directed Crystallisation of Synthetic Polymers by Low-Molar-Mass Self-Assembled Templates *Macromolecular Rapid Comm.* **24** 496-502

Nogales A., Mitchell G.R., Vaughan A.S (2003) Anisotropic crystallization in polypropylene induced by deformation of a nucleating agent network Macromolecules **36** 4898-4906

Nogales A., Thornley S.A, and Mitchell G.R. (2004) Shear cell for in-situ WAXS, SAXS and SANS experiments on polymer melts under flow fields *J Macromol Sci-Physics* **B43** 1161-1170

Nogales A., Olley R.H. and Mitchell G.R. (2016) On Morphology of row structures in polyethylene generated by shear alignment of dibenzylidene sorbitol Submitted *to Journal of Polymer Research*

Okesola BO, Vieira VMP, Cornwell DJ, Whitelaw NK and Smith DK. (2015), 1,3:2,4-Dibenzylidene-D-sorbitol (DBS) and its derivatives – efficient, versatile and industrially relevant low-molecular-weight gelators with over 100 years of history and a bright future, *Soft Matter*, 11, 4768–4787

Olley R.H., Mitchell G.R., and Moghaddam Y. 2014 On Row-Structures in Sheared Polypropylene and a Propylene-Ethylene Copolymer *European Polymer Journal* 53 37-49

Pople J.A., Mitchell G.R., Sutton S.J., Vaughan A.S. and Chai C. 1999The development of organised structures in polyethylene crystallised from a sheared melt, analyzed by WAXS and TEM *Polymer* **40** 2769-2777

Sangeetha NM and Maitra U (2005) Supramolecular gels: Functions and uses, *Chem. Soc. Rev*., 34, 821-836

Siripitayananon J., Wangsoub S, Olley R.H., Mitchell G.R. (2004) The use of a low-molar-mass self-assembled template to direct the crystallisation of poly (epsilon-caprolactone) Macromolecular Rapid Comm 25, 1365-1370

Smith DK. (2009), Lost in translation? Chirality effects in the self-assembly of nanostructured gel-phase materials, *Chem. Soc. Rev*., 38, 684-694.

Terech P and Weiss RG. (1997), Low Molecular Mass Gelators of Organic Liquids and the Properties of Their Gels,, *Chem. Rev*., 97 (8), 3133–3160

Tuffen, H, James, M, Castro, J & Schipper, CI 2013, 'Exceptional mobility of an advancing rhyolitic obsidian flow at Cordon Caulle volcano in Chile: observations from Cordón Caulle, Chile, 2011-2013.' *Nature Communications*, vol 4, 2709., 10.1038/ncomms3709

Van Driessche AES, García-Ruíz JM, Tsukamoto K, Patiño-Lopez LD and Satoh H. (2011), Ultraslow growth rates of giant gypsum crystals, *PNAS* 108 15721–15726

Wangsoub S, Olley R.H. and Mitchell G.R. (2005) Directed Crystallisation of Poly(e caprolactone) Using a Low-molar-mass Self-assembled Template Macromol Chem Phys 206 1826-1839

Wangsoub S, Davis FJ, Mitchell GR and Olley RH. (2008), Enhanced Templating in the Crystallisation of Poly(ε-caprolactone) using 1,3:2,4-di(4-chlorobenzylidene) sorbitol, *Macromol. Rapid Commun*., 2008, 29, 1861–1865

Wangsoub S., Davis F.J., Harris P.J.F, Mitchell G.R and Olley R.H. (2016) Structure and Morphology of high liquid content gels formed from alkanes and dibenzylidene sorbitol Submitted to Physical Chemistry, chemical Physics.

Wangsoub S. and Mitchell G.R. (2009) Shear controlled crystal size definition in a low molar mass compound using a polymeric solvent Soft Matter, 5, 525

Wangsoub S. Olley R.H. and Mitchell G.R. (2016) Templating the crystallisation of polyethylene using dibenzylidene sorbitol Submitted to Macromolecular chemistry and Physics

Watase M and Itagaki H (1998), Thermal and Rheological Properties of Physical Gels Formed From Benzylidene-D-Sorbitol Derivatives", *Bull. Chem. Soc. Jpn* 71(6), 1457-1466

Yamasaki S and Tsutsumi H. (1994), Microscopic Studies of 1,3 : 2,4-Di-O-benzylidene-D-sorbitol in Ethylene Glycol, *Bull. Chem. Soc. Jpn*., 67, 906-911.

Yamasaki S and Tsutsumi H. (1995), The Dependence of the Polarity of Solvents on 1,3 : 2,4-Di-*o*-benzylidene-D-sorbitol Gel, *Bull. Chem. Soc. Jpn*., 68,123-127

Yamasaki S, Ohashi Y, Tsutsumi H and Tsujii K. (1995), The Aggregated Higher-Structure of 1,3 : 2,4-Di-*o*-benzylidene-D-sorbitol in Organic Gels, *Bull. Chem. Soc. Jpn*., 68,146-151

Zweifel H. (2001), *Plastics Additives Handbook* ed. Hanser Chapter 18.